Frustrated quantum Heisenberg double-tetrahedral and octahedral chains at high magnetic fields

Olesia Krupnitska
Institute for Condensed Matter Physics, National Academy of Sciences of Ukraine, Svientsitskii Street 1, 79011 L'viv, Ukraine

(Received 4 April 2019; revised 16 July 2020; accepted 20 July 2020; published 5 August 2020)

We consider the spin-1/2 antiferromagnetic Heisenberg model on two one-dimensional frustrated lattices, a double-tetrahedral chain and an octahedral chain, with almost dispersionless (flat) lowest magnon band in a strong magnetic field. Using the localized-magnon picture, we construct an effective description of the one-dimensional chains with triangle and square traps within the strong-coupling approximation. We perform extensive exact diagonalization and density matrix renormalization group calculations to check the validity of the obtained effective Hamiltonians by comparison with the initial models with special focus on the magnetization and specific heat at high magnetic fields.

DOI: 10.1103/PhysRevB.102.064403

I. INTRODUCTION

The study of frustrated quantum Heisenberg antiferromagnets remains a hot topic in condensed matter physics [1,2]. This special class of frustrated quantum Heisenberg antiferromagnets, which have a dispersionless (flat) band in the one-magnon energy spectrum, is of great interest, since such systems can be mapped on the classical lattice gas of hard-core objects (see, e.g., a recent review [3]). In previous studies it was shown that the high-field low-temperature properties of such spin systems can be studied in detail within the localized-magnon approach [4–6]. The theory developed in Refs. [4–6] works perfectly well in the case of so-called perfect geometry, when the one-magnon states are strictly localized, i.e., the one-magnon band is strictly dispersionless. Moreover, the ground-state characteristic features of such spin systems are a plateau and a jump to the saturation in the magnetization curve [4], the spin-Peierls instability [7], and the residual entropy at the saturation field [5,6]. However, in real systems, the conditions that provide a strict localization of magnons can be violated and a theory of almost flat-band systems is necessary.

The effects of small deviation from ideal flat-band geometry were studied in Refs. [8–13]. In particular, to study high-field low-temperature properties of initial deformed one- or two-dimensional frustrated Heisenberg antiferromagnets, effective Hamiltonians were constructed using the localized-magnon approach. In the present work, we propose a systematic theory for some other systems near the flat-band point. To be specific, we consider two frustrated quantum spin lattices in a strong magnetic field, the double-tetrahedral chain and the octahedral chain (see Fig. 1). These frustrated lattices were studied previously in the literature by various authors. In particular, the double-tetrahedral chain, which can be understood as a one-dimensional analog of the pyrochlore antiferromagnet, was studied in Refs. [14–21]. Exact ground and excited states of an antiferromagnetic quantum octahedral chain were studied in Refs. [22–24] and low-temperature thermodynamics or quantum phase transitions of octahedral chains were investigated in Refs. [25,26].

It is important to note that double-tetrahedral geometry is realized for the spin system of Cu^{2+} ions in the magnetic compound $Cu_3Mo_2O_9$ [27–29]. As shown in Refs. [27–29], the exchange-interaction network of this compound comprises spin-1/2 antiferromagnetic uniform chains J_4 and antiferromagnetic dimers J_3 which are the main determinants of the magnetism. The exchange interactions J_1 and J_2 connect the chains and dimers. A set of exchange-interaction parameters J_1–J_4 were estimated from the experimental data and have the following values: $J_4 = 6.5$ meV ≈ 75.43 K, $J_3 = 5.7$ meV ≈ 66.15 K, and $J_1 - J_2 = 3.06$ meV ≈ 35.51 K [29]. It is worth noting that there is a whole class of geometrically frustrated compounds based on cobalt oxide, $R\mathrm{BaCo_4O_7}$ with a rare earth atom R, which has swedenborgite lattice structure [30]. Considering one columnar stripe in such a magnetic compound, we could single out a double-tetrahedral chain structure. On the other hand, the solid-state realization of the octahedral spin chain has not been found yet, but spin clusters with the geometric shape of an octahedron can be found in polynuclear complexes such as Cu_6 [31] or V_6 [32]. We believe that our theoretical findings could be useful in the synthesis of the solid realization of the octahedral spin chain by experimentalists.

In what follows, we consider the spin-1/2 antiferromagnetic Heisenberg model on a double-tetrahedral chain and an octahedral chain (see Fig. 1) in a magnetic field with the Hamiltonian

$$H = \sum_{(ij)} J_{ij}\mathbf{s}_i \cdot \mathbf{s}_j - hS^z, \quad S^z = \sum_{i=1}^{N} s_i^z. \tag{1.1}$$

Here the first sum runs over all nearest neighbors on a lattice, whereas the second one runs over all N lattice sites. Note that $[S^z, H] = 0$, i.e., the eigenvalues of S^z are good quantum numbers. To accomplish a description of the model, we introduce a convenient labeling of the lattice sites by a pair of indices, where the first number enumerates the cells ($m = 1, \ldots, \mathcal{N}$, $\mathcal{N} = N/4$ for the double-tetrahedral chain or $\mathcal{N} = N/5$ for the octahedral chain, and N is the number of sites) and the second one enumerates the position of the site within the

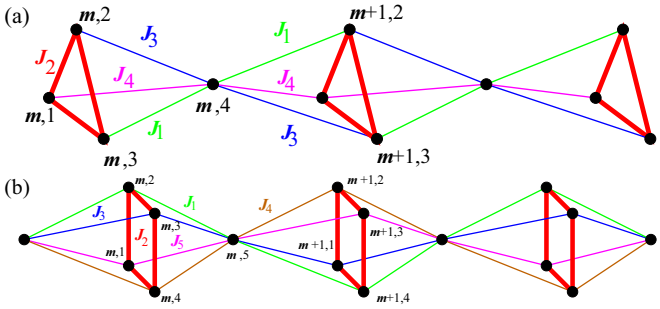

FIG. 1. The schematic of (a) the double-tetrahedral chain and (b) the octahedral chain described by Hamiltonian (1.1).

cell (see Fig. 1). Both these models may support independent localized-magnon states, which dominate their high-field low-temperature thermodynamics. A localized magnon state can be located within a trapping cell (equilateral triangle or square) due to destructive quantum interference. It has the lowest energy in the subspace $S^z = N/2 - 1$ if the strength of the antiferromagnetic bonds of the trapping cells J_2 exceeds a lower bound [4]. Owing to the localized nature of these states the many-magnon ground state can be constructed by filling the traps by localized magnons. Moreover, magnon localization occurs due to the specific lattice geometry and hence requires a certain relation between the exchange interactions J_{ij}. For the considered traps (triangle or square) this condition is fulfilled if an arbitrary bond of the trapping cell and the surrounding bonds attached to the two sites of this bond form an isosceles triangle, i.e., $J_i = J$ $(i \neq 2)$ in Fig. 1. In the present study we deal with the case when the localization conditions are slightly violated.

In previous investigations it was shown, that localized states on trapping cells with even numbers of sites (vertical bond for diamond or dimer-plaquette chains, square for square-kagome lattice) have a nondegenerate ground state for the one-particle problem [8–10]. A new interesting feature concerns the frustrated double-tetrahedral chain. In general, lattices with odd sites in trapping cells have an additional degree of freedom—chirality [33]—which leads to increasing of the degeneracy of the ground state of the double-tetrahedral chain. That is why one of the main goals of the present research is to develop a systematic theory not only in the case of distorted lattice geometry but also in the presence of an additional degree of freedom in the system, namely, chirality.

The paper is organized as follows. In Sec. II we construct effective Hamiltonians for the double-tetrahedral chain and the octahedral chain in a strong magnetic field within the strong-coupling approximation. In Sec. III we compare exact diagonalization and density matrix renormalization group results for the initial and the corresponding effective models to estimate the validity of the obtained effective models and discuss the magnetization process and temperature dependence of specific heat. We summarize our findings in Sec. IV.

II. EFFECTIVE HAMILTONIANS: STRONG-COUPLING APPROACH

To study the low-energy behavior of the introduced models we use a strong-coupling perturbation theory. For considered systems one can easily single out a regular pattern of $\mathcal{N}$ trapping cells which do not have common sites and have sufficiently large couplings J_2 (the squares for the octahedral chain or the equilateral triangles for the double-tetrahedral chain). The traps are joined via weaker connecting bonds J_i $(i \neq 2)$, which in the ideal geometry case prevent the escape of the localized magnons from the traps.

Within the strong-coupling approach one assumes that the coupling J_2 is the dominant one, i.e., $J_i/J_2 \ll 1$ $(i \neq 2)$. At high fields only a few states of the trapping cell are relevant, namely, the fully polarized state $|u\rangle$ and the localized-magnon state $|d\rangle$; in the case of the triangular trap there are two localized-magnon states $|d+\rangle$ and $|d-\rangle$ with different chiralities. All other sites $m, 4$ or $m, 5$ $(m = 1, \ldots, \mathcal{N})$ have fully polarized spins. As the magnetic field decreases from very large values, the ground state of the trap undergoes a transition between the state $|u\rangle$ and the state $|d\rangle$ at the "bare" saturation field h_0. The Hamiltonian H is split into a "main" part H_{main} (the Hamiltonian of all traps and the Zeeman interaction of all spins with the magnetic field h_0) and a perturbation $V = H - H_{\text{main}}$. The ground state $|\varphi_0\rangle$ of the Hamiltonian without the connecting bonds $J_i = 0$ $(i \neq 2)$ and at $h - h_0 = 0$ is $2^{\mathcal{N}}$-fold degenerate for the case of the octahedral chain and $3^{\mathcal{N}}$-fold degenerate in the case of the double-tetrahedral chain. These ground states form a model subspace defined by the projector $P = |\varphi_0\rangle\langle\varphi_0|$. When J_i $(i \neq 2)$ and $h - h_0$ deviate from zero we are interested in an effective Hamiltonian H_{eff} which acts on the model space only but gives the exact ground-state energy. H_{eff} can be found perturbatively [34–36] and is given by

$$H_{\text{eff}} = PHP + PV \sum_{\alpha \neq 0} \frac{|\varphi_\alpha\rangle\langle\varphi_\alpha|}{\varepsilon_0 - \varepsilon_\alpha} VP + \cdots . \tag{2.1}$$

Here $|\varphi_\alpha\rangle$ $(\alpha \neq 0)$ are excited states of H_{main}. To rewrite the effective Hamiltonian in a more transparent form amenable for further analysis it might be convenient to introduce (pseudo)spin operators representing the states of each trapping cell.

A. Heisenberg double-tetrahedral chain

A new feature in the case of the double-tetrahedral chain is related to the chirality [33] of the triangle. As a result, in a strong magnetic field for each triangle we consider three states:

$$\begin{aligned} |u\rangle &= |\uparrow\uparrow\uparrow\rangle, \\ |d+\rangle &= \frac{1}{\sqrt{3}}(|\downarrow\uparrow\uparrow\rangle + \omega|\uparrow\downarrow\uparrow\rangle + \omega^2|\uparrow\uparrow\downarrow\rangle), \\ |d-\rangle &= \frac{1}{\sqrt{3}}(|\downarrow\uparrow\uparrow\rangle + \omega^2|\uparrow\downarrow\uparrow\rangle + \omega|\uparrow\uparrow\downarrow\rangle), \\ \omega &= e^{i\frac{2\pi}{3}}. \end{aligned} \tag{2.2}$$

Their energies are $3J_2/4 - 3h/2$, $-3J_2/4 - h/2$, and $-3J_2/4 - h/2$, respectively. The saturation field is $h_0 = 3J_2/2$. If $h = h_0$ and $J_1 = J_3 = J_4 = 0$ the ground state of H, $|\varphi_0\rangle$, is $3^{\mathcal{N}}$-fold degenerate. The projector onto the

ground states of $H_{\rm main}$ is

$$P = |\varphi_0\rangle\langle\varphi_0| = \otimes_m P_m,$$
$$P_m = ((|u\rangle\langle u| + |d+\rangle\langle d+| + |d-\rangle\langle d-|) \otimes |\uparrow_4\rangle\langle\uparrow_4|)_m. \tag{2.3}$$

Evidently, we face a spin-1 problem. We use the following representation for the (pseudo)spin-1 operators:

$$T^x = \frac{1}{\sqrt{2}}\begin{pmatrix} 0 & 1 & 0 \\ 1 & 0 & 1 \\ 0 & 1 & 0 \end{pmatrix}, \quad T^y = \frac{1}{i\sqrt{2}}\begin{pmatrix} 0 & 1 & 0 \\ -1 & 0 & 1 \\ 0 & -1 & 0 \end{pmatrix},$$
$$T^z = \begin{pmatrix} 1 & 0 & 0 \\ 0 & 0 & 0 \\ 0 & 0 & -1 \end{pmatrix}. \tag{2.4}$$

Let us put

$$|d+\rangle\langle d+| \to \begin{pmatrix} 1 \\ 0 \\ 0 \end{pmatrix}\begin{pmatrix} 1 & 0 & 0 \end{pmatrix} = \begin{pmatrix} 1 & 0 & 0 \\ 0 & 0 & 0 \\ 0 & 0 & 0 \end{pmatrix} = \frac{1}{2}\left(T^z + T^{z2}\right),$$
$$|u\rangle\langle u| \to \begin{pmatrix} 0 & 0 & 0 \\ 0 & 1 & 0 \\ 0 & 0 & 0 \end{pmatrix} = 1 - T^{z2},$$
$$|d-\rangle\langle d-| \to \begin{pmatrix} 0 & 0 & 0 \\ 0 & 0 & 0 \\ 0 & 0 & 1 \end{pmatrix} = \frac{1}{2}\left(-T^z + T^{z2}\right). \tag{2.5}$$

We have to notice here that such an encoding contradicts the intuitive expectation that "the fully polarized state corresponds to $T^z = +1$." According to the introduced correspondence, the fully polarized state corresponds to $T^z = 0$. Indeed, while s is real spin which interacts with the magnetic field, **T** is a pseudospin which simply represents three states of the triangle.

The chirality operator for a triangle in the double-tetrahedral chain was introduced in previous work [19] as

$$\chi_m = \frac{4}{\sqrt{3}}(\mathbf{s}_{m,1} \cdot [\mathbf{s}_{m,2} \times \mathbf{s}_{m,3}]) \tag{2.6}$$

and it was shown that $\chi_m|d+\rangle_m = |d+\rangle_m$, $\chi_m|d-\rangle_m = -|d-\rangle_m$. Moreover, this operator can be expressed in terms of states $|d+\rangle$, $|d-\rangle$ as

$$\chi_m = |d+\rangle\langle d+|_m - |d-\rangle\langle d-|_m, \tag{2.7}$$

that coincides with the T^z_m operator.

Then the first term in Eq. (2.1) can be written in the terms of (pseudo)spin-1 operators:

$$PHP = P\sum_{m=1}^{\mathcal{N}}\left(-2h + \frac{3}{4}J_2 + \frac{3J}{2} + (h - h_1)T^{z2}_m\right)P,$$
$$h_1 = \frac{3}{2}J_2 + J, \quad J = \frac{J_1 + J_3 + J_4}{3}. \tag{2.8}$$

For the ideal geometry case this is the well-known result [19].

Relevant excited states contain only one flipped spin on the site connecting two neighboring triangles. The energy of these excited states is $\varepsilon_0 + h_0$ with $h_0 = 3J_2/2$ and therefore for the second term in Eq. (2.1) we have

$$PV\sum_{\alpha\neq 0}\frac{|\varphi_\alpha\rangle\langle\varphi_\alpha|}{\varepsilon_0 - \varepsilon_\alpha}VP = -\frac{2}{3J_2}\sum_{m=1}^{\mathcal{N}}P\left(\frac{J_4}{2}s^-_{m,1} + \frac{J_3}{2}s^-_{m,2} + \frac{J_1}{2}s^-_{m,3}\right.$$
$$\left. + \frac{J_4}{2}s^-_{m+1,1} + \frac{J_1}{2}s^-_{m+1,2} + \frac{J_3}{2}s^-_{m+1,3}\right)$$
$$\times\left(\frac{J_4}{2}s^+_{m,1} + \frac{J_3}{2}s^+_{m,2} + \frac{J_1}{2}s^+_{m,3}\right.$$
$$\left. + \frac{J_4}{2}s^+_{m+1,1} + \frac{J_1}{2}s^+_{m+1,2} + \frac{J_3}{2}s^+_{m+1,3}\right)P. \tag{2.9}$$

After the evaluation of all necessary matrix elements $Ps^{\mp}_{m,i}P$, we get

$$PV\sum_{\alpha\neq 0}\frac{|\varphi_\alpha\rangle\langle\varphi_\alpha|}{\varepsilon_0 - \varepsilon_\alpha}VP = -\frac{1}{18J_2}\sum_{m=1}^{\mathcal{N}}P((a|d+\rangle + a^*|d-\rangle)\langle u|_m$$
$$+ (a^*|d+\rangle + a|d-\rangle)\langle u|_{m+1})$$
$$\times(|u\rangle(a^*\langle d+| + a\langle d-|)_m$$
$$+ |u\rangle(a\langle d+| + a^*\langle d-|)_{m+1})P. \tag{2.10}$$

Here

$$a = J_4 + \omega^2 J_3 + \omega J_1 = |a|e^{i\alpha},$$
$$|a| = \sqrt{J_1^2 + J_3^2 + J_4^2 - J_1J_4 - J_1J_4 - J_3J_4}. \tag{2.11}$$

Using (pseudo)spin-1 T^α_m operators, we have the following expression for the effective Hamiltonian:

$$H_{\rm eff} = \sum_{m=1}^{\mathcal{N}}\left[C + \left(h - h_1 - \frac{|a|^2}{9J_2}\right)T^{z2}_m - \frac{1}{18J_2}\left[(a^2 + a^{*2})\left(T^{x2}_m - T^{y2}_m\right)\right.\right.$$
$$+ \frac{1}{2}\left((a - a^*)^2\left(T^z_mT^x_mT^x_{m+1}T^z_{m+1} + T^x_mT^z_mT^z_{m+1}T^x_{m+1}\right) + (a + a^*)^2\left(T^z_mT^y_mT^y_{m+1}T^z_{m+1} + T^y_mT^z_mT^z_{m+1}T^y_{m+1}\right)\right.$$
$$\left.\left. + i(a^{*2} - a^2)\left(T^z_mT^x_mT^y_{m+1}T^z_{m+1} + T^x_mT^z_mT^z_{m+1}T^y_{m+1}\right) + i(a^2 - a^{*2})\left(T^z_mT^y_mT^x_{m+1}T^z_{m+1} + T^y_mT^z_mT^z_{m+1}T^x_{m+1}\right)\right)\right]\Bigg],$$
$$C = -2h + \frac{3}{4}J_2 + \frac{3J}{2}, \quad h_1 = \frac{3}{2}J_2 + J, \quad J = \frac{J_1 + J_3 + J_4}{3}, \quad a = J_4 + \omega^2 J_3 + \omega J_1, \quad \omega = e^{i\frac{2\pi}{3}}. \tag{2.12}$$

This result can be also written in more compact matrix notation:

$$H_{\rm eff}=\sum_{m=1}^{\mathcal{N}}\Bigg[C\begin{pmatrix}1&0&0\\0&1&0\\0&0&1\end{pmatrix}+\begin{pmatrix}h-h_1&0&0\\0&0&0\\0&0&h-h_1\end{pmatrix}_m-\frac{1}{18J_2}\Bigg(\begin{pmatrix}2|a|^2&0&a^2+a^{*2}\\0&0&0\\a^2+a^{*2}&0&2|a|^2\end{pmatrix}_m$$
$$+\frac{1}{2}\begin{pmatrix}0&a&0\\0&0&0\\0&a^*&0\end{pmatrix}_m\begin{pmatrix}0&0&0\\a&0&a^*\\0&0&0\end{pmatrix}_{m+1}+\frac{1}{2}\begin{pmatrix}0&0&0\\a^*&0&a\\0&0&0\end{pmatrix}_m\begin{pmatrix}0&a^*&0\\0&0&0\\0&a&0\end{pmatrix}_{m+1}\Bigg)\Bigg],$$
$$C=-2h+\frac{3}{4}J_2+\frac{3J}{2},\quad h_1=\frac{3}{2}J_2+J,\quad J=\frac{J_1+J_3+J_4}{3},\quad a=J_4+\omega^2J_3+\omega J_1,\quad \omega=e^{i\frac{2\pi}{3}}. \tag{2.13}$$

The obtained effective Hamiltonian acts in the space of $3^{\mathcal{N}}$ ground states of $H_{\rm main}$ and corresponds to the unfrustrated (pseudo)spin-1 chain in the magnetic field. For the ideal geometry case, i.e., when $J_1=J_3=J_4$ ($J_4+\omega^2J_3+\omega J_1=0$), we have noninteracting (pseudo)spins 1 in a magnetic field and obtained effective model (2.13) commutes with scalar chirality operator (2.7). It is important to notice that for the distorted geometry case the chirality operator (2.7) commutes only with terms in effective model (2.13) which are proportional to T_m^{z2} and this means that deviation from the ideal geometry leads to breaking of chiral symmetry.

B. Heisenberg octahedral chain

In the case of the octahedral chain the following two states of each square are relevant in a strong magnetic field:

$$|u\rangle=|\uparrow\uparrow\uparrow\uparrow\rangle,$$
$$|d\rangle=\tfrac{1}{2}(|\uparrow\uparrow\uparrow\downarrow\rangle-|\uparrow\uparrow\downarrow\uparrow\rangle+|\uparrow\downarrow\uparrow\uparrow\rangle-|\downarrow\uparrow\uparrow\uparrow\rangle). \tag{2.14}$$

Their energies are J_2-2h and $-J_2-h$, respectively. For the projector onto the ground-state manifold of $H_{\rm main}$ we have

$$P=|\varphi_0\rangle\langle\varphi_0|=\otimes_m P_m,$$
$$P_m=\left((|u\rangle\langle u|+|d\rangle\langle d|)\otimes|\uparrow_5\rangle\langle\uparrow_5|\right)_m. \tag{2.15}$$

Similar to the double-tetrahedral chain, the set of relevant excited states $|\varphi_\alpha\rangle$ ($\alpha\neq0$) is the set of the states with only one flipped spin $|\downarrow_5\rangle$ on those sites which connect two neighboring squares J_2. Using (pseudo)spin-1/2 operators for each cell,

$$1=|u\rangle\langle u|+|d\rangle\langle d|,\quad T^z=\tfrac{1}{2}(|u\rangle\langle u|-|d\rangle\langle d|),$$
$$|u\rangle\langle u|=\tfrac{1}{2}+T^z,\quad |d\rangle\langle d|=\tfrac{1}{2}-T^z, \tag{2.16}$$

Eq. (2.1) becomes

$$H_{\rm eff}=\sum_m\left(C-\mathsf{h}T_m^z-\mathsf{J}\left(T_m^xT_{m+1}^x+T_m^yT_{m+1}^y\right)\right),$$
$$C=-2h+J_2+\frac{3}{2}J-\frac{(J_1-J_3+J_4-J_5)^2}{16J_2},$$
$$\mathsf{h}=h-h_1-\frac{(J_1-J_3+J_4-J_5)^2}{8J_2}, \tag{2.17}$$
$$\mathsf{J}=\frac{(J_1-J_3+J_4-J_5)^2}{16J_2}.$$

The obtained effective Hamiltonian in the strong-coupling approach acts in the space of two ground states of $H_{\rm main}$ and corresponds to an unfrustrated spin-1/2 isotropic XY chain in a transverse magnetic field [37]. Therefore, the free energy (per cell) of the initial frustrated quantum spin model in the low-temperature strong-field regime for $\mathcal{N}\to\infty$ is given by

$$f(T,h)=\mathsf{C}-\frac{T}{2\pi}\int_{-\pi}^{\pi}d\kappa\,\ln\left(2\cosh\frac{\Lambda_\kappa}{2T}\right) \tag{2.18}$$

with

$$\Lambda_\kappa=\mathsf{h}+\mathsf{J}\cos(\kappa). \tag{2.19}$$

Knowing the free energy (2.18), one can easily obtain all thermodynamic quantities. For example, the magnetization per cell is given by $M(T,h)=-\partial f(T,h)/\partial h$, and the specific heat $C(T,h)$ can be found as $C(T,h)=-T\partial^2f(T,h)/\partial T^2$ [the magnetization per site and specific heat are five times smaller: $m(T,h)=M(T,h)/5$, $c(T,h)=C(T,h)/5$)]. In the case of the ideal geometry, i.e., when $J_1=J_3=J_4=J_5$, we face noninteracting (pseudo)spins 1/2 in a magnetic field.

III. HIGH-FIELD LOW-TEMPERATURE THERMODYNAMICS

In this section we verify the region of validity of the obtained effective Hamiltonians (2.13) and (2.17). To check the quality of the obtained effective description we perform exact diagonalization (ED) and density matrix renormalization group (DMRG) calculations [38]. We consider initial chains with periodic boundary conditions ($N=4\mathcal{N}=16$ for the double-tetrahedral chain and $N=5\mathcal{N}=15$ for the octahedral chain) in ED calculations or open chains with $\mathcal{N}=60$ in DMRG calculations and compute the magnetization $m(T,h)$ at low temperatures and the specific heat $c(T,h)$ at high fields. Periodic boundary conditions are applicable to systems with a small number of sites to ensure the equivalence of all sites. This reduces the volume of computations by reducing the Hilbert dimension of the entire system. We have used the DMRG method to expand our chain length beyond the exact limit. The most important difference from other numerical methods is that DMRG prefers open boundary conditions and in the present study it is used for the zero-temperature condition. In the evaluation of magnetization curves by the DMRG method we used the control parameters sweeps = 4 and maxstates = 100. Results for the initial full model (1.1) are compared with corresponding data for effective models.

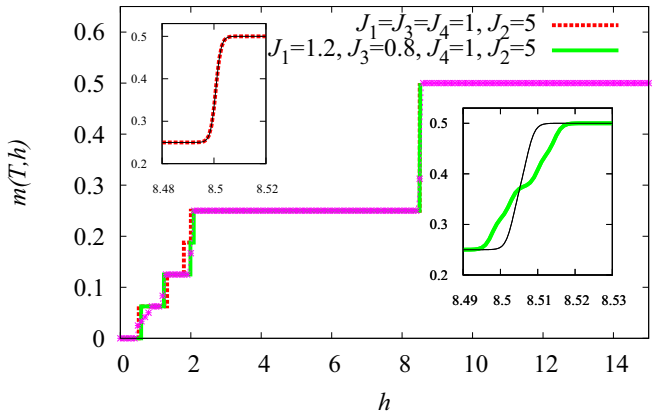

FIG. 2. Field dependencies of the magnetization (per site) $m(T, h)$ of the double-tetrahedral chain for ideal ($J_1 = J_3 = J_4 = 1$, $J_2 = 5$, red dotted line, left inset) and deformed geometry ($J_1 = 1.2$, $J_2 = 5$, $J_3 = 0.8$, $J_4 = 1$, green thick line, right inset) of the lattice. ED data for the initial model ($N = 16$) are compared with corresponding data for the effective model ($\mathcal{N} = 4$, thin black lines). DMRG data obtained for $\mathcal{N} = 60$, i.e., $N = 240$ (magenta symbols).

In main panels of Figs. 2 and 3 we show the total magnetization curves at zero temperature for the considered models of $N = 16$ (the double-tetrahedral chain, Fig. 2) and $N = 15$ (the octahedral chain, Fig. 3). In these figures dotted red curves indicate the ED results for ideal geometry and thick solid green and blue curves denote the ED results for slightly distorted geometry; magenta symbols indicate the DMRG results for initial deformed models; thin black curves indicate the results for effective models. The magnetization curves demonstrate the existence of plateaus, which are a characteristic feature of localized magnons, at one-third of the saturation magnetization in the case of the double-tetrahedral

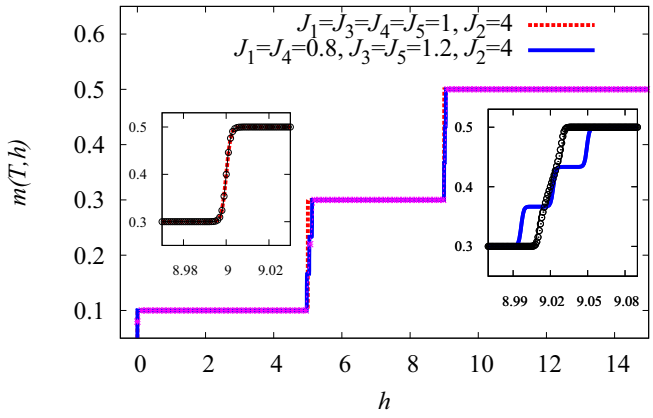

FIG. 3. Field dependencies of the magnetization (per site) $m(T, h)$ of the octahedral chain for ideal ($J_1 = J_3 = J_4 = 1 = J_5$, $J_2 = 4$, red dotted line, left inset) and deformed geometry ($J_1 = J_4 = 0.8$, $J_3 = J_5 = 1.2$, $J_2 = 4$, blue thick line, right inset) of the lattice. ED data for the initial model ($N = 15$) are compared with corresponding data for the effective model ($\mathcal{N} = 3$, thin black lines). DMRG data obtained for $\mathcal{N} = 60$, i.e., $N = 300$ (magenta symbols). Effective-model predictions for thermodynamically large chains are denoted by open black circles.

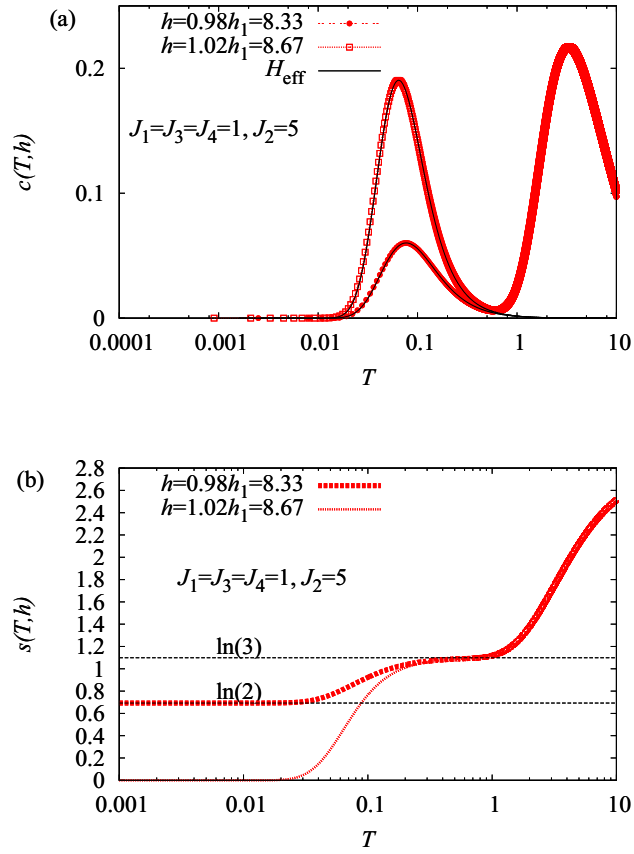

FIG. 4. Temperature dependencies of (a) the specific heat (per site) $c(T, h)$ and (b) the entropy (per cell) $s(T, h)$ of the double-tetrahedral chain for ideal ($J_1 = J_3 = J_4 = 1$, $J_2 = 5$) geometry of the lattice. ED data for the initial model ($N = 16$) are compared with corresponding data for the effective model ($\mathcal{N} = 4$, thin black curves).

chain (Fig. 2) and at one-fifth and three-fifths of the saturation magnetization for the octahedral chain (Fig. 3). Insets demonstrate the influence of finite temperature, i.e., $T = 0.001$, on magnetization and also show the region of applicability of the constructed effective theory for ideal and distorted geometry of the lattice. To be specific, the left insets in Figs. 2 and 3 demonstrate the strict jump of magnetization to the saturation value for the ideal double-tetrahedral and octahedral chains. Comparing the results of ED calculations for initial (dotted red curves) and effective models (thin black curves) for ideal chains indicates their excellent agreement. The right insets in Figs. 2 and 3 show how these the strict jumps modify due to small deviations from the ideal geometry.

In Figs. 4(a), 5(a), and 6 we also show the temperature dependencies of the specific heat at high magnetic fields for ideal (red symbols) and slightly distorted geometries (green and blue symbols). Temperature dependencies of the entropy of ideal and distorted double-tetrahedral chains in strong magnetic field are depicted in Figs. 4(b) and 5(b). Results for the corresponding effective models [see Eqs. (2.13) and (2.17)] are denoted by thin black curves. The results of Jordan-Wigner fermionization for the effective model for the octahedral chain are denoted by black open circles in

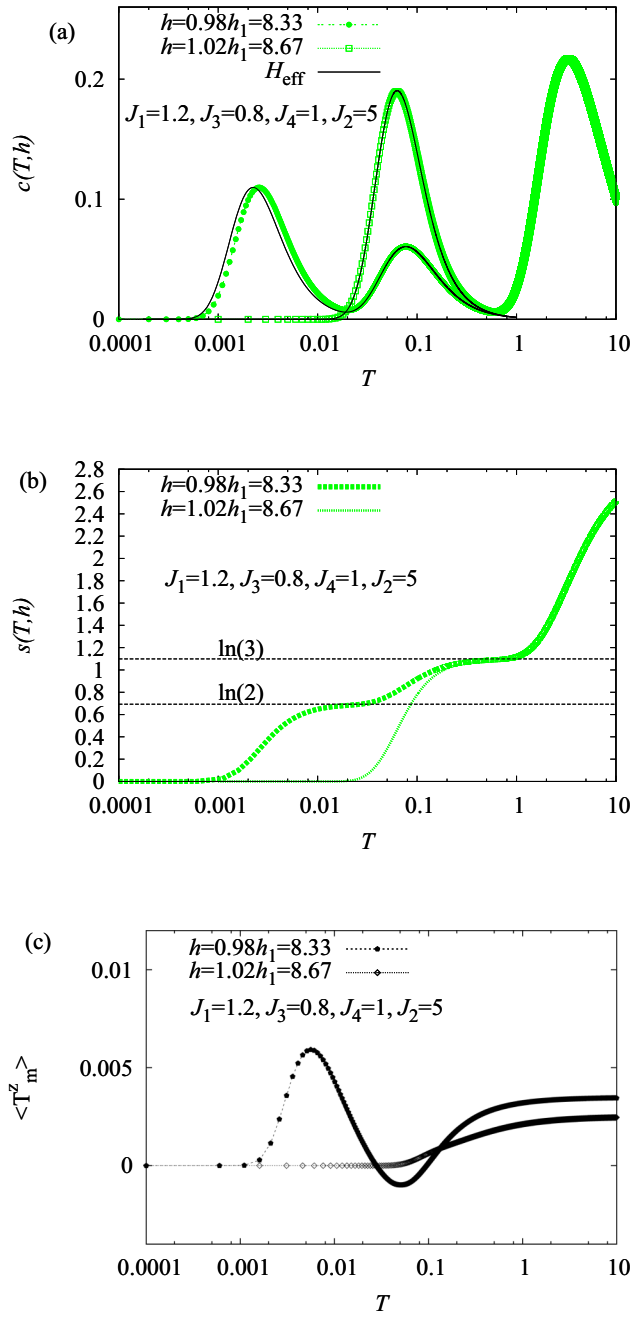

FIG. 5. Temperature dependencies of (a) the specific heat (per site) $c(T, h)$ and (b) the entropy (per cell) $s(T, h)$ of the double-tetrahedral chain for deformed geometry ($J_1 = 1.2, J_2 = 5, J_3 = 0.8$, $J_4 = 1$) of the lattice. ED data for the initial model ($N = 16$) are compared with corresponding data for the effective model ($\mathcal{N} = 4$, thin black curves). (c) Thermal average of the chirality operator (2.7) for the distorted double-tetrahedral chain.

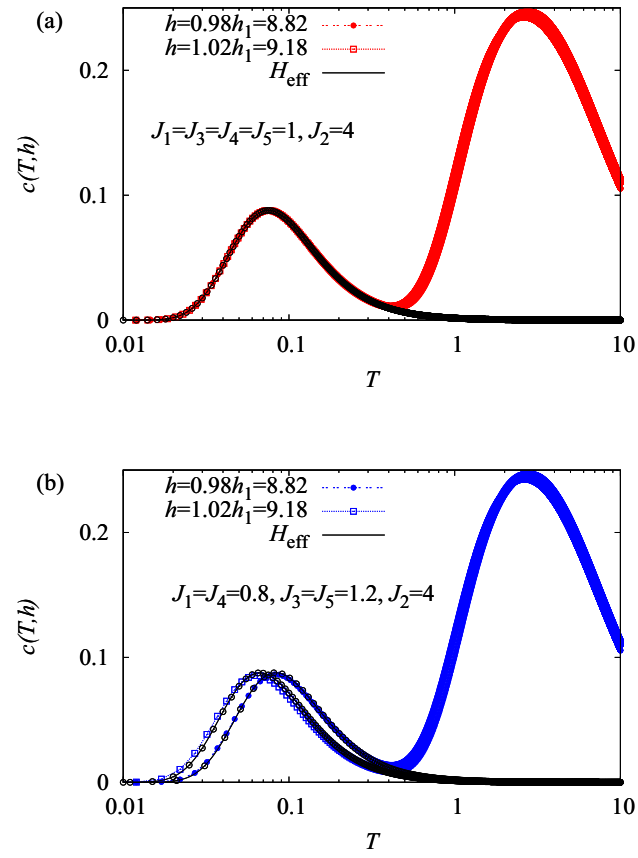

FIG. 6. Temperature dependencies of the specific heat (per site) $c(T, h)$ of the octahedral chain for (a) ideal ($J_1 = J_3 = J_4 = J_5 = 1$, $J_2 = 4$, red symbols) and (b) deformed geometry ($J_1 = J_4 = 0.8$, $J_3 = J_5 = 1.2$, $J_2 = 4$, blue symbols) of the lattice. ED data for the initial model ($N = 15$) are compared with corresponding data for the effective model ($\mathcal{N} = 3$, thin black lines). Effective-model predictions for thermodynamically large chains are denoted by empty black circles.

Figs. 3 and 6. The thermal average of the chirality operator (2.7) for the distorted double-tetrahedral chain in a magnetic field below the saturation value is depicted in Fig. 5(c).

Now we can discuss generic features, which arise as the consequence of small deviation from the perfect geometry of the lattice. First of all, deviation from the ideal geometry does not affect the noticeable change in width of the plateau preceding the jump of magnetization to saturation (see Figs. 2 and 3), but has an essential influence on the magnetization jump present for the ideal geometry. As one can see from right insets in Figs. 2 and 3, deviation from the ideal geometry together with finite temperature leads to the smearing of the jump to saturation in the magnetization curve, which is another prominent feature of localized magnons both for the double-tetrahedral and the octahedral chains. For deformed initial chains the agreement between the effective theory given in Eqs. (2.13) and (2.17) and the exact-diagonalization data become worse. The constructed effective theory within the strong-coupling approximation reproduces the low-temperature behavior of magnetization in the vicinity of the saturation field only qualitatively and underestimates the width of the region where the low-temperature magnetization shows a steep increase between two plateau values.

As one can see from Figs. 4(a) and 6(a), specific heat demonstrates a two-peak structure, which is typical for ideal geometry both for the double-tetrahedral and the octahedral chains. The low-temperature peak of the specific heat corresponds to the energy scale set by the degenerated manifold of states being ground states at magnetic fields near the saturation. Moreover, such a characteristic extra low-

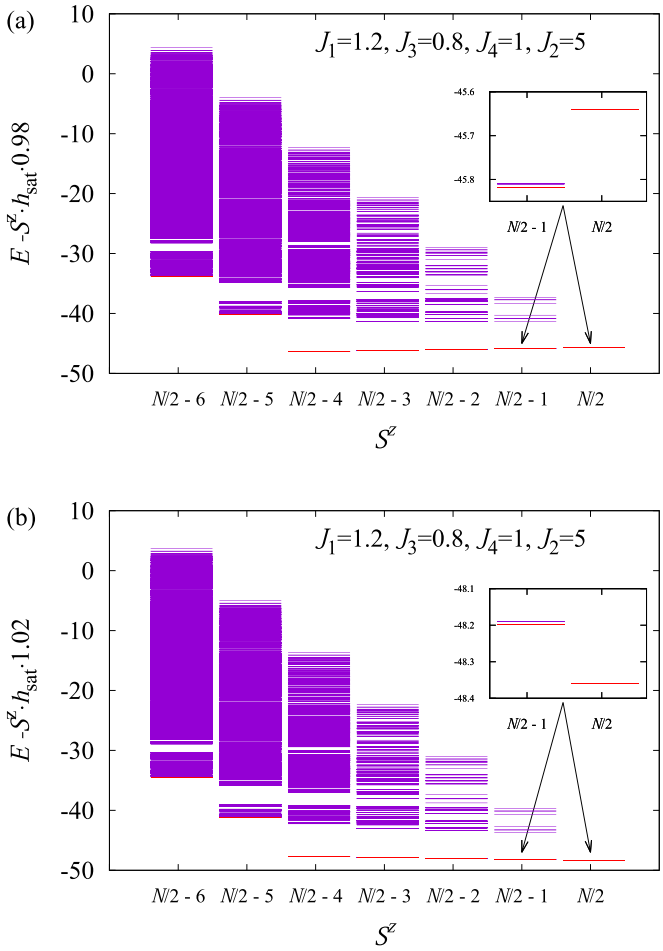

FIG. 7. Energy levels of the distorted double-tetrahedral chain ($J_1 = 1.2$, $J_2 = 5$, $J_3 = 0.8$, $J_4 = 1$) in the subspaces with different value of S^z operator in a magnetic field (a) slightly below the saturation value (b) just above the saturation value.

temperature peak in the specific heat survives in distorted systems. In the case of the double-tetrahedral chain, deviation from ideal geometry leads to the lifting of the degeneracy due to the chirality degrees of freedom and one of the twofold degenerate flat bands in the energetic spectrum acquires a small dispersion. As a result, the temperature dependence of the specific heat of a deformed double-tetrahedral chain in a magnetic field slightly below saturation value demonstrates a three-peak structure [see Fig. 5(a)]. It should be noted that such a three-peak structure of the specific heat appears exclusively at high magnetic fields just below the saturation value. The confirmation of this statement can be understood from the energy levels of the deformed double-tetrahedral chain in subspaces with different values of the operator S^z, $S^z = \frac{N}{2}, \frac{N}{2} - 1, \ldots$, which are shown in Fig. 7. In a magnetic field a bit under the saturation value in subspace, for example, one flipped spin($S^z = \frac{N}{2} - 1$) system has degenerate low-lying excitations from the ground state to first-excited states. Such excited states are ground states in a magnetic field below the saturation [see Fig. 7(a)]. There are also a lot of low-lying excitations in other subspaces with smaller eigenvalues of the total spin $S^z \geqslant \frac{N}{2} - \mathcal{N}$, which are closely related to nearly flat-band states differing in chirality. To emphasize the contribution of the chirality degree of freedom let us consider the temperature dependence of chirality operator (2.7). We find from Fig. 5(c) that in magnetic fields below the saturation value chirality not only plays a crucial role, but it obviously has certain correlations with observed maximums of the specific heat. However, when the magnetic field is above the saturation value [see Fig. 7(b)] those states are not ground states anymore and therefore do not contribute to the specific heat at very low temperature. On the other hand, the explanation of the appearance of an additional low-temperature peak in the specific heat can be understood from the temperature dependence of the entropy of the double-tetrahedral chain in a strong magnetic field [see Figs. 4(b) and 5(b)]. In the case of the ideal geometry of the double-tetrahedral chain ($J_1 = J_3 = J_4 = 1$, $J_2 = 5$) the high degeneracy of the localized eigenstates leads to a residual ground-state entropy in a magnetic field a bit below the saturation, $S(h = 0.98h_{\rm sat}) = \ln(2)$, which stems from the chiral degree of freedom. The deviation from ideal geometry of the lattice eliminates the degeneracy of the ground states and the temperature dependence of the entropy acquires a three-peak shape. Moreover, the appearance of an additional low-temperature peak in the specific heat can be interpreted from a symmetry viewpoint: deviation from ideal geometry leads to explicit breaking of a discrete Z_2 symmetry of the unit cell (tetrahedron) of the double-tetrahedral chain, while in the case of the ideal lattice geometry such breaking symmetry is not present. An effective Hamiltonian is capable of reproducing not only the low-temperature peak of the specific heat (ideal and deformed octahedral chains and ideal double-tetrahedral chain), but also the second peak in the specific heat of the deformed double-tetrahedral chain [see Figs. 4(a), 5(a), and 6]. However, the constructed effective theory concerns the low-temperature physics, and therefore does not reproduce the high-temperature maximum of the specific heat for both Heisenberg chains considered in this paper.

IV. CONCLUSIONS

In conclusion, we have examined the high-field low-temperature properties of the spin-1/2 Heisenberg model on the double-tetrahedral and octahedral chains both for ideal and distorted geometry of the lattice. Using the concept of localized magnons and a strong-coupling approximation we proposed an effective theory to explain the low-temperature thermodynamics of the considered systems in a high magnetic field. It was shown that the presence of an additional degree of freedom of trapping cells in the double-tetrahedral chain, i.e., chirality, leads to increasing degeneracy of one-magnon states and these states differ by chirality values. An effective description of the double-tetrahedral chain at high magnetic field corresponds to an unfrustrated spin-1 chain with nearest-neighbor interactions in a magnetic field while the octahedral chain is described by the exactly solvable spin-1/2 isotropic XY chain in a magnetic field. Moreover, the obtained effective Hamiltonians are much simpler than the initial ones: they are free of frustration, have a smaller number of sites, and refer to the reduced Hilbert space. New features which appear due to small deviation from ideal geometry at strong magnetic

fields are (i) the smearing of the perfect jump to the saturation in the magnetization curve for both deformed chains and (ii) lifting of the degeneracy due to chirality degrees of freedom on a triangle and the appearance of the additional peak in the specific heat of the distorted double-tetrahedral chain in a magnetic field just below the saturation value.

The developed approach can be also adapted to other frustrated quantum Heisenberg antiferromagnets with spin higher than $1/2$ and extended to the case of low magnetic fields. It is necessary to choose the dominant states with the least energy in the vicinity of zero magnetic field and repeat all required calculations to construct an effective Hamiltonian. However, the aim of the present investigation concerns the high-field regime, where manifestation of almost localized magnons is the most striking.

It is worth noting that $Cu_3Mo_2O_9$ [27–29] can be presented as a double-tetrahedral chain, but with a different deformation type than was considered here. The construction of an effective theory in the case of the deformation of equilateral triangles will be a task for future study.

ACKNOWLEDGMENTS

The author would like to thank O. Derzhko, T. Krokhmalskii, T. Verkholyak, and J. Strečka for invaluable discussions and comments. The present study was partially supported by the National Academy of Sciences of Ukraine under a Grant for the Research groups of young scientists (Contract No. 7/2019) and by Grant of the President of Ukraine (Contract No. F82/221-2019).

[1] G. Misguich and C. Lhuillier, in *Frustrated Spin Systems*, edited by H. T. Diep (World Scientific, Singapore, 2013), pp. 229–306; J. Richter, J. Schulenburg, and A. Honecker, in *Quantum Magnetism*, Lecture Notes in Physics Vol. 645, edited by U. Schollwöck, J. Richter, D. J. J. Farnell, and R. F. Bishop (Springer, Berlin, 2004), pp. 85–153.

[2] M. Takigawa and F. Mila, in *Introduction to Frustrated Magnetism: Materials, Experiments, Theory*, edited by C. Lacroix, P. Mendels, and F. Mila (Springer, Berlin, 2011), p. 241.

[3] O. Derzhko, J. Richter, and M. Maksymenko, Int. J. Mod. Phys. B **29**, 1530007 (2015).

[4] J. Schnack, H.-J. Schmidt, J. Richter, and J. Schulenburg, Eur. Phys. J. B **24**, 475 (2001); J. Schulenburg, A. Honecker, J. Schnack, J. Richter, and H.-J. Schmidt, Phys. Rev. Lett. **88**, 167207 (2002).

[5] M. E. Zhitomirsky and H. Tsunetsugu, Phys. Rev. B **70**, 100403(R) (2004); Prog. Theor. Phys. Suppl. **160**, 361 (2005).

[6] O. Derzhko and J. Richter, Phys. Rev. B **70**, 104415 (2004); Eur. Phys. J. B **52**, 23 (2006).

[7] J. Richter, O. Derzhko, and J. Schulenburg, Phys. Rev. Lett. **93**, 107206 (2004).

[8] O. Derzhko, J. Richter, O. Krupnitska, and T. Krokhmalskii, Phys. Rev. B **88**, 094426 (2013).

[9] O. Derzhko, J. Richter, O. Krupnitska, and T. Krokhmalskii, Fiz. Nizk. Temp. (Kharkiv) **40**, 662 (2014) [Low Temp. Phys. **40**, 513 (2014)].

[10] J. Richter, O. Krupnitska, T. Krokhmalskii, and O. Derzhko, J. Magn. Magn. Mater. **379**, 39 (2015).

[11] O. Derzhko, O. Krupnitska, B. Lisnyi, and J. Strečka, Europhys. Lett. **112**, 37002 (2015).

[12] O. Krupnitska, J. Richter, and O. Derzhko, Acta Phys. Pol. A **132**, 1234 (2017).

[13] J. Richter, O. Krupnitska, V. Baliha, T. Krokhmalskii, and O. Derzhko, Phys. Rev. B **97**, 024405 (2018).

[14] M. Mambrini, J. Trébosc, and F. Mila, Phys. Rev. B **59**, 13806 (1999).

[15] O. Rojas and F. C. Alcaraz, Phys. Rev. B **67**, 174401 (2003).

[16] C. D. Batista and B. S. Shastry, Phys. Rev. Lett. **91**, 116401 (2003).

[17] D. Antonosyan, S. Bellucci, and V. Ohanyan, Phys. Rev. B **79**, 014432 (2009).

[18] M. Maksymenko, O. Derzhko, and J. Richter, Acta Phys. Pol. A **119**, 860 (2011).

[19] M. Maksymenko, O. Derzhko, and J. Richter, Eur. Phys. J. B **84**, 397 (2011).

[20] L. Gálisová and J. Strečka, Phys. Rev. E **91**, 022134 (2015).

[21] L. Gálisová, Physica B: Condensed Matter **536**, 498 (2018).

[22] I. Bose, J. Phys.: Condens. Matter **1**, 9267 (1989).

[23] I. Bose, J. Phys.: Condens. Matter **2**, 5479 (1990).

[24] I. Bose, Phys. Rev. B **45**, 13072 (1992).

[25] J. Strečka, J. Richter, O. Derzhko, T. Verkholyak, and K. Karľová, Phys. Rev. B **95**, 224415 (2017).

[26] J. Strečka, J. Richter, O. Derzhko, T. Verkholyak, and K. Karľová, Physica B **536**, 364 (2018).

[27] M. Hase, H. Kitazawa, K. Ozawa, T. Hamasaki, H. Kuroe, and T. Sekine, J. Phys. Soc. Jpn. **77**, 034706 (2008).

[28] H. Kuroe, T. Hosaka, S. Hachiuma, T. Sekine, M. Hase, K. Oka, T. Ito, H. Eisaki, M. Fujisawa, S. Okubo, and H. Ohta, J. Phys. Soc. Jpn. **80**, 083705 (2010).

[29] M. Matsumoto, H. Kuroe, T. Sekine, and M. Hase, J. Phys. Soc. Jpn. **81**, 024711 (2012).

[30] S. Buhrandt and L. Fritz, Phys. Rev. B **90**, 094415 (2014).

[31] C. W. Liu, C.-M. Hung, B. Kumar Santra, J.-Ch. Wang, H.-M. Kao, and Zh. Lin, Inorg. Chem. **42**, 8551 (2003).

[32] C. Daniel and H. Hart, J. Am. Chem. Soc. **127**, 13978 (2005).

[33] W. J. Caspers and G. I. Tielen, Physica A **135**, 519 (1986); X. G. Wen, F. Wilczek, and A. Zee, Phys. Rev. B **39**, 11413 (1989); J. Richter, *ibid.* **47**, 5794 (1993).

[34] D. J. Klein, J. Chem. Phys. **61**, 786 (1974).

[35] P. Fulde, in *Electron Correlations in Molecules and Solids* (Springer-Verlag, Berlin, 1993), p. 77.

[36] F. H. L. Essler, H. Frahm, F. Göhmann, A. Klümper, and V. E. Korepin, *The One-Dimensional Hubbard Model* (Cambridge University Press, Cambridge, U.K., 2005), p. 38.

[37] E. Lieb, T. Schultz, and D. Mattis, Ann. Phys. (NY) **16**, 407 (1961); S. Katsura, Phys. Rev. **127**, 1508 (1962); **129**, 2835 (1963).

[38] A. F. Albuquerque *et al.* (ALPS Collaboration), J. Magn. Magn. Mater. **310**, 1187 (2007); B. Bauer *et al.* (ALPS Collaboration), J. Stat. Mech. (2011) P05001.